Polímeros
ISSN 1678-5169 (Online)

https://doi.org/10.1590/0104-1428.20240133

ORIGINAL ARTICLES

Optimizing graphene-enhanced polycaprolactone nanofibers for superior biomedical properties

Sankar Thangavel[1]*, Kannan Thanneerpanthalpalayam Kandasamy[2], Rajasekar Rathanasamy[3] and Ratchagaraja Dhairiyasamy[4,5]

[1]Department of Mechanical Engineering, Paavai College of Engineering, Namakkal, Tamilnadu, India
[2]Department of Mechanical Engineering, Jerusalem College of Engineering, Chennai, Tamil Nadu, India
[3]Department of Mechanical Engineering, Kongu Engineering College, Erode, Tamilnadu, India
[4]Department of Electronics and Communication Engineering, Saveetha School of Engineering, Saveetha Institute of Medical and Technical Sciences, Saveetha University, Chennai, Tamilnadu, India
[5]Centre of Research Impact and Outcome, Chitkara University, Rajpura, Punjab, India
**ersankar.t@gmail.com*

Abstract

Electrospun polycaprolactone (PCL) nanofibers are widely studied for biomedical applications due to their biodegradability and processability, but their limited mechanical strength and bioactivity restrict advanced use. This study addresses these challenges by incorporating four types of functionalized graphene—carboxyl (CFG), hydroxyl (HFG), amine (AFG), and sulfonic (SFG)—into PCL at varying concentrations. Nanocomposite fibers were fabricated via electrospinning and characterized using SEM, FTIR, Raman, DSC, TGA, tensile testing, and MTT assay. Among all, PCL reinforced with 1 wt% SFG showed superior properties, including a tensile strength of 5.8 MPa, 34% thermal residue at 600°C, and 93% cell viability at 72 hours, outperforming pure PCL by over 60% in strength and 9% in biocompatibility. The enhancement is attributed to improved dispersion and strong interfacial bonding from polar functional groups. These results highlight the potential of functionalized graphene to engineer high-performance nanofibers for tissue engineering and regenerative medicine applications.

Keywords: *PCL nanocomposites, electrospinning, graphene, mechanical properties, biocompatibility.*

Data Availability: Research data is available upon request from the corresponding author.

How to cite: Thangavel, S., Kandasamy, K. T., Rathanasamy, R., & Dhairiyasamy, R. (2025). Optimizing graphene-enhanced polycaprolactone nanofibers for superior biomedical properties. *Polímeros: Ciência e Tecnologia*, *35*(4), e20250042. https://doi.org10.1590/0104-1428.20240133

1. Introduction

The increasing demand for advanced biomaterials has prompted significant interest in nanotechnology-driven approaches to develop next-generation scaffolds for biomedical applications. Among various nanostructured platforms, electrospun polymeric nanofibers have gained considerable attention due to their structural similarity to natural extracellular matrices, which promotes cellular adhesion, proliferation, and differentiation. Electrospinning technology offers the advantage of producing continuous nanofibers with high surface-to-volume ratios, tunable porosity, and the capacity to incorporate functional additives, making it an ideal tool for fabricating scaffolds for tissue engineering, wound dressings, and drug delivery systems[1]. However, the full potential of electrospun scaffolds relies heavily on the selection and engineering of suitable polymeric systems with enhanced mechanical, thermal, and biological properties.

Polycaprolactone (PCL) is a semicrystalline, aliphatic polyester widely recognized for its biodegradability, non-toxic degradation byproducts, and compatibility with human tissue. Its low melting temperature and solubility in a range of organic solvents make it particularly attractive for electrospinning. Nevertheless, pure PCL suffers from inherent limitations such as low tensile strength, slow degradation rate, and insufficient bioactivity, restricting its applicability in mechanically demanding or rapidly healing tissues[2]. Various modification strategies have been proposed to overcome these drawbacks, including polymer blending, surface functionalization, and the incorporation of nanofillers. Among them, reinforcement with carbon-based nanomaterials has shown great promise in enhancing the structural and functional attributes of PCL nanofibers[3].

Graphene and its derivatives have emerged as superior nanofillers due to their exceptional electrical, thermal, and mechanical properties, as well as their large surface area and tunable surface chemistry. Functionalized graphene, particularly those modified with oxygen-containing groups such as carboxyl (–COOH), hydroxyl (–OH), amine ($–NH_2$), or sulfonic acid ($–SO_3H$), has demonstrated improved dispersibility in polymer matrices and stronger interfacial bonding [4]. These functional groups are known

to form hydrogen bonds or electrostatic interactions with polymer chains, enhancing filler-matrix compatibility and promoting stress transfer across the interface. Furthermore, graphene-based nanocomposites have been reported to exhibit antibacterial activity and support cellular behaviors critical for tissue regeneration, making them ideal candidates for biomedical scaffolding[5].

The reviewed literature (Table 1) confirms that electrospinning is a versatile and effective method for fabricating nanocomposite fibers with improved properties. Several studies emphasize the role of graphene and other nanofillers in enhancing thermal stability, mechanical strength, and structural uniformity. However, few works systematically evaluate the impact of different functional groups (e.g., –COOH, –OH, $–NH_2$, $–SO_3H$) on fiber properties or include biocompatibility assessments[16]. The current study bridges this gap by comparing four functionalized graphene derivatives in a unified PCL matrix, revealing the superior reinforcement and biological response offered by AFG and SFG systems, which have received minimal attention in past biomedical research.

Previous research has explored the incorporation of graphene oxide (GO) or reduced graphene oxide (rGO) into PCL matrices, with results indicating improvements in mechanical strength, thermal stability, and biological response. However, most of these studies have been limited to a single form of graphene derivative, often lacking comparative analysis across different functional groups[17]. Moreover, limited attention has been given to systematically optimizing the graphene content to balance mechanical reinforcement with dispersion quality and cytocompatibility. Without this optimization, the tendency of graphene to agglomerate at higher concentrations can negate its beneficial effects, leading to inconsistent fiber morphology and compromised performance. Additionally, few investigations have examined the role of newer functional groups such as sulfonic or amine moieties in modifying PCL-based nanofibers.

To fill these gaps, the current research focuses on the design and optimization of electrospun PCL nanofibers reinforced by chemically prepared graphene derivatives like (CFG), (HFG), (AFG) and (SFG). It was possible with such tailored graphene derivatives to introduce diverse chemical complements, which control dispersion dynamics, interfacial bonding, and final performance qualities of the nanocomposite fibers. The investigation includes changing the ratio of graphene to 0.5 wt%, 1 wt%, and 2 wt% to determine the optimal loading of the filler for every derivative at the aspects of morphological stability, mechanical properties, thermal performance, and biological safety[18].

This research aims to prepare and evaluate multifunctional nanofiber mats from PCL and graphene derivatives prepared by electrospinning for selecting the best mixture providing mechanical, thermal and biological performance. SEM, FTIR, Raman spectroscopy, DSC, TGA, tensile testing, and MTT assay analyze the nanocomposites. Using such analytical methods, we can analyze such parameters as fiber morphology, intermolecular forces, graphene integration, as well as biocompatibility with HDFs to enable a comprehensive analysis of the structure–property–function correlations in the fabricated nanocomposites[19].

The novelty of the present study lies in the simultaneous exploration and comparison of four distinct functionalized graphene derivatives within a unified experimental framework. Unlike previous studies that focused on GO or rGO alone, this research highlights the unique contributions of less-explored derivatives like AFG and SFG, revealing their superior influence on fiber refinement and reinforcement. The inclusion of these

Table 1. Comparative literature summary of polymer-based nanocomposite fibers prepared via electrospinning.

Nanofiller Type	Electrospinning Used	Focus Application	Fiber Morphology	Thermal Stability	Mechanical Strength	Biocompatibility	Relevance to Current Study
TiO_2, epoxy	Yes	Superhydrophobic coatings	↓ (bead formation, rough)	↔	↔	Not tested	Reinforces the role of nanofillers in wettability and morphology enhancement[6]
Hydroxyapatite	Yes	Bone regeneration	↑ (fibrous, uniform)	↑	↑	↑	Demonstrates the role of mineral fillers for cytocompatibility—parallels with HFG[7]
Fe_3O_4@AuNPs	Yes	Catalysis & magnetic recyclability	↑ (hierarchical nanostructure)	↑	↔	Not tested	Highlights multifunctionality potential of electrospun nanofibers[8]
Functionalized GO (NH_2-POSS)	Yes	Thermal applications	↑ (dense, aligned)	↑↑	↑	Not tested	Directly supports current use of NH_2-GO (AFG) for thermal/mechanical tuning[9]
MXene@AgNP	Yes	Wastewater treatment	↑ (intercalated flakes)	↑	↔	Not tested	Reinforces the benefit of dispersion strategy to avoid agglomeration[10]
GO–COOH@AgNPs	Yes	Photocatalysis	↑ (dense, ultrafine)	↑	↔	Not tested	Supports the effectiveness of COOH functional groups for composite performance[11]
CuO, Al, GO	Yes	Energetic materials	↑ (smooth, uniform)	↑↑	↑	Not tested	Highlights the impact of 0.5 wt% GO on fiber quality and reaction enhancement[12]
Graphene	Yes	Electronics	↑ (mesh-like)	↑	↑	Not tested	Validates fiber alignment and graphene's effect on conductivity and thermal properties[13]
Graphene, Fe_3O_4	Yes	Magnetic fiber fabrication	↑ (aligned via magnetic/electric field)	↔	↔	Not tested	Highlights innovative alignment strategies—applicable to scaffold orientation[14]
$BaTiO_3$	Yes	Dielectric materials	↑ (dispersed, low loss)	↔	↑	Not tested	Shows electrospinning's role in nanofiller dispersion and matrix enhancement[15]

derivatives is particularly significant, as they introduce highly polar or reactive functional groups capable of forming stronger intermolecular interactions with PCL chains. The observed improvements in fiber uniformity, tensile strength, and thermal degradation resistance establish these nanofillers as viable candidates for high-performance biomedical applications. Moreover, the use of a standardized electrospinning protocol ensures that the effects of functional group chemistry and filler concentration can be directly compared across formulations, strengthening the study's internal consistency[20].

The outcomes of this research are expected to contribute valuable insights into the rational design of advanced nanofiber-based scaffolds for biomedical engineering. By demonstrating the synergistic effects of functionalized graphene with tailored surface chemistry, the study offers new possibilities for enhancing the mechanical and biological performance of electrospun nanocomposites. In particular, the findings may benefit the development of tissue engineering scaffolds with improved load-bearing capability, wound dressings with prolonged stability and antibacterial function, and drug delivery systems with extended degradation profiles. The study's systematic approach to filler optimization and functional group evaluation represents a forward step in creating customizable nanomaterials for diverse clinical applications[21].

This work responds to a critical need for multifunctional and high-performance biomaterials by developing electrospun PCL nanofibers reinforced with various functionalized graphene derivatives. Through comparative analysis and optimization of graphene content, the study establishes structure–property relationships that govern the mechanical, thermal, and biological behavior of the resulting nanocomposites. The inclusion of underexplored functional groups such as $–NH_2$ and $–SO_3H$ introduces new perspectives on filler design, while the comprehensive characterization strategy ensures robust evaluation of material performance. The knowledge gained from this research can inform future innovations in polymer nanocomposite development for biomedical applications, thereby advancing the field toward more effective and personalized medical solutions.

2. Materials and Methods

The base polymer used in the present study was polycaprolactone (PCL), a widely employed biodegradable aliphatic polyester. It was procured from Sigma-Aldrich with an average molecular weight of 80,000 g/mol. Its known advantages such as biocompatibility, processability, and biodegradation suitability, make it ideal for biomedical applications. In order to enhance the performance of PCL, it was reinforced with functionalized graphene derivatives. Specifically, two forms of chemically functionalized graphene were selected: carboxyl-functionalized graphene (CFG) and hydroxyl-functionalized graphene (HFG). These derivatives were purchased from Graphene Supermarket and featured a purity of 99% with particle sizes ranging from 1 to 10 µm. Their functional groups were chosen to improve dispersion within the polymer and increase interaction at the filler–matrix interface. In later extensions of the study, amine-functionalized graphene (AFG) and sulfonic-functionalized graphene (SFG) were incorporated to provide a comparative perspective of functionality-induced enhancements[22].

To prepare the electrospinning solution, PCL was dissolved in a solvent blend composed of chloroform and N,N-dimethylformamide (DMF) in a 4:1 volume ratio. The polymer concentration was maintained at 12 wt% to ensure appropriate viscosity and conductivity for stable jet formation during electrospinning. The graphene derivatives were first dispersed in DMF by probe sonication for 60 minutes at 100 W to reduce agglomeration. This step was critical to achieve exfoliation of graphene sheets and homogeneous nanofiller distribution. After ultrasonication, the dispersed nanofiller solution was gradually added to the pre-prepared PCL solution, followed by magnetic stirring for 4 hours at 500 rpm. An additional ultrasonication step of 30 minutes was then conducted to further reduce any micro-agglomerates and promote complete dispersion. The mixtures were prepared at three concentrations—0.5 wt%, 1.0 wt%, and 2.0 wt%—for each graphene derivative to systematically investigate the effect of nanofiller loading on the morphology and performance of the resulting nanofibers.

The electrospinning apparatus consisted of a programmable syringe pump, a 21-gauge needle connected to a high-voltage power supply, and a grounded rotating drum collector. The optimized electrospinning parameters included an applied voltage of 15 kV, a feed rate of 1 mL/h, and a fixed distance of 15 cm between the needle tip and the collector. The drum rotation speed was kept low to fabricate randomly oriented fibers. All electrospinning procedures were conducted at ambient room temperature under controlled humidity conditions. Fibers were collected continuously for four hours per sample onto aluminum foil-wrapped collectors. After deposition, the fiber mats were dried at room temperature for 24 hours to ensure the complete removal of residual solvents. This setup is illustrated in Figure 1, which depicts the electrospinning assembly and process flow.

To ensure experimental reliability and repeatability, all samples were prepared in triplicate (n = 3). For characterization studies such as FTIR, SEM, Raman, DSC, and tensile testing, a minimum of three independent measurements were obtained from different regions of each sample. For tensile properties, five replicates were tested per group (n = 5), and for MTT assay-based biocompatibility tests, both biological and technical replicates (n = 3 × 3) were employed at each time point.

Morphological characterization was conducted using a JEOL JSM-IT200 scanning electron microscope to evaluate the surface structure and fiber formation in the electrospun mats. Prior to SEM imaging, all nanofiber samples were gold-sputtered under vacuum to eliminate surface charging and ensure image clarity. Imaging was carried out at magnifications ranging from 5000x to 10000x to capture detailed features of fiber morphology. From each micrograph, the fiber diameter was quantitatively analyzed using ImageJ software by measuring 100 randomly selected fibers per image, enabling statistically robust assessment of the average diameter and distribution. Figures present SEM micrographs of electrospun PCL nanofibers reinforced with carboxyl-functionalized graphene (CFG) at concentrations of 0.5 wt%, 1.0 wt%, and 2.0 wt%. The images demonstrate how increasing CFG content alters the fiber characteristics in terms of surface smoothness, structural uniformity, and average thickness[23].

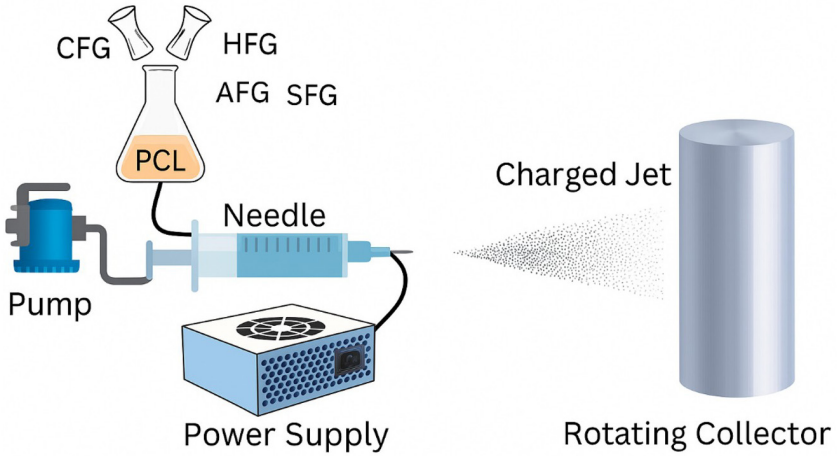

Figure 1. Electrospinning process setup.

In addition, SEM images were obtained for nanofibers containing h(HFG), (AFG), and (SFG), each at a loading of 1 wt%. These are displayed in Figures, which enable direct comparison of the effects of different functional groups on fiber formation. The SFG-reinforced fibers exhibited the most refined morphology, with the smallest average diameter and highly uniform structure, attributed to enhanced dispersion and interfacial bonding. Fibers containing AFG and HFG showed improved structure compared to unreinforced PCL but with slightly larger diameters and minor variations in alignment, indicating moderate interaction and dispersion levels.

To further visualize the influence of both graphene content and functional group type on fiber diameter, comparative fiber diameter plots were prepared. This analysis highlights a consistent reduction in average fiber diameter with increasing nanofiller concentration up to 1 wt%, followed by a slight increase at 2 wt%, likely due to nanoparticle agglomeration. All graphene types showed the lowest diameter at 1 wt%, confirming this as the optimal concentration for achieving uniform, fine nanofiber morphology.

(FTIR) was conducted to verify the successful incorporation of functionalized graphene into the PCL matrix and to examine possible chemical interactions. Spectra were recorded in the range of 4000 to 400 cm^{-1} using a Bruker Tensor 27 spectrometer. Peaks corresponding to the ester bond (C=O at 1720 cm^{-1}), CH_2 stretching vibrations (~2945 and 2865 cm^{-1}), and C–O–C stretching (~1100–1240 cm^{-1}) were analyzed. Any changes in peak intensity or position were attributed to hydrogen bonding or electrostatic interaction between the graphene functional groups and the polymer chains. The FTIR spectra for all samples are presented[24].

Raman spectroscopy was employed to confirm the structural presence and dispersion quality of graphene within the PCL matrix. Spectra were collected using a 532 nm excitation laser with a spectral resolution of 1 cm^{-1}. Key bands, including the D-band (~1350 cm^{-1}), G-band (~1580 cm^{-1}), and the 2D-band (~2700 cm^{-1}), were monitored. The relative intensity ratio of D to G bands (I_D/I_G) was calculated to assess defect levels in functionalized graphene. Raman mapping further validated the spatial uniformity of the filler across the nanofiber surface[25].

The mechanical properties of the electrospun nanofiber mats were evaluated using an Instron 5567 universal testing machine with a 100 N load cell. Samples were cut into rectangular strips (5 mm × 30 mm), and tensile testing was performed at a crosshead speed of 5 mm/min. Young's modulus, ultimate tensile strength, and elongation at break were determined for each sample type. These properties were statistically averaged across five specimens per group. The tensile performance of all compositions is summarized graphically.

Thermal stability and crystallinity of the samples were assessed using differential scanning calorimetry (DSC) and thermogravimetric analysis (TGA). DSC analysis was carried out under nitrogen from 25°C to 100°C at a heating rate of 10°C/min. The melting temperature (Tm), crystallization temperature (Tc), and degree of crystallinity were calculated from endothermic peak areas. TGA was conducted under nitrogen with a temperature ramp from 30°C to 600°C at 10°C/min to determine the onset of thermal degradation and residual weight percentage. TGA results for 1 wt% nanocomposites are shown[26].

To evaluate the cytocompatibility of the nanofiber mats, an in vitro MTT assay was performed using human dermal fibroblasts (HDFs). Electrospun mats were UV-sterilized and placed in 24-well plates, where HDFs were seeded at a density of 1×10^4 cells/well. The cells were incubated at 37°C in a humidified CO_2 environment and assessed at 24, 48, and 72 hours post-seeding. At each time point, the MTT reagent was added, and after incubation, formazan crystals were dissolved in DMSO and absorbance was measured at 570 nm using a microplate reader. The procedure allowed quantification of cell viability and proliferation, which was used to infer the biocompatibility of each nanocomposite formulation.

All materials and methods adopted in this study were selected to ensure the fabrication of high-performance nanofibrous mats with potential for biomedical applications. The stepwise optimization of each variable—from solvent system and filler dispersion to electrospinning conditions and biological testing—ensured consistency and reproducibility

across the experiments. The full experimental matrix, including sample composition, test types, and replicates, was implemented to guarantee the scientific rigor required for biomaterial development[27].

SEM images (Figure 2) reveal the influence of functionalized graphene derivatives on the morphology of electrospun polycaprolactone (PCL) nanofibers. Pure PCL nanofibers serve as the baseline, displaying a smooth, bead-free surface with an average diameter of approximately 620 nm and a randomly oriented fiber network. Upon incorporation of 0.5 wt% carboxyl-functionalized graphene (CFG), a noticeable reduction in fiber diameter is observed (~580 nm), along with the development of slight surface texture, suggesting early-stage polymer-filler interaction and enhanced solution conductivity. At 1 wt% CFG, the fiber morphology is optimized, exhibiting thinner, more uniform fibers with an average diameter around 520 nm. This reflects the improved alignment and chain stretching attributed to the hydrogen bonding and electrostatic interactions offered by carboxyl groups. However, increasing the CFG content to 2 wt% results in partial agglomeration, as evidenced by a marginal increase in diameter (~610 nm) and less regular fiber arrangement, likely due to increased viscosity and nanoparticle clustering disrupting the electrospinning jet[28].

Hydroxyl- and sulfonic-functionalized graphene (HFG and SFG), the effect of functional group chemistry becomes more distinct. PCL nanofibers with 0.5 wt% HFG show a modest decrease in diameter (~570 nm), similar to CFG at the same loading, but with a slightly rougher fiber texture. At 1 wt% HFG, the morphology improves further with an average diameter of approximately 510 nm, though still not as refined as CFG, reflecting the relatively weaker interaction strength of hydroxyl groups. With 2 wt% HFG, aggregation effects become evident, leading to larger, less uniform fibers (~600 nm) and minor surface irregularities. In contrast, nanofibers containing 1 wt% sulfonic-functionalized graphene (SFG) display the most refined morphology, with the thinnest diameter (~495 nm) and highly uniform, smooth fibers. The strong ionic nature of sulfonic groups enhances dispersion and interfacial bonding, resulting in superior electrospinning stability and fiber alignment.

The SEM images confirm that both the type and concentration of graphene derivatives significantly influence fiber morphology. The optimal morphology is observed at 1 wt% loading, with SFG providing the most effective reinforcement, followed by CFG and HFG. These morphological improvements support the enhancements seen in mechanical and thermal performance, validating the role of surface-functionalized graphene in engineering advanced nanofiber scaffolds.

Figure 3 shows the variation in fiber diameter of electrospun polycaprolactone (PCL) nanofibers reinforced with different types of functionalized graphene—(CFG), h(HFG), (AFG), and (SFG)—across three graphene concentrations: 0.5 wt%, 1.0 wt%, and 2.0 wt%. The graph highlights the morphological response of the fibers to nanoparticle loading and surface chemistry[29].

At 0 wt%, the baseline fiber diameter for pure PCL is approximately 620 nm. With the introduction of graphene, the fiber diameter decreases across all derivatives, reaching a minimum at 1.0 wt%. Specifically, PCL/SFG shows the lowest average diameter at this concentration (~495 nm), which corresponds to a 20.2% reduction compared to pure PCL. This is followed by AFG (~500 nm), HFG (~510 nm), and CFG (~520 nm), suggesting that highly polar and reactive groups like $–SO_3H$ and $–NH_2$ enhance solution conductivity and polymer chain alignment, thereby producing finer fibers.

At 2.0 wt%, a reversal trend is observed, with the diameters increasing again. This likely indicates the onset of graphene agglomeration at higher concentrations, which disrupts the homogeneity and viscosity of the spinning solution. Still, even at 2.0 wt%, SFG and AFG retain a 5.6–6.5% smaller fiber

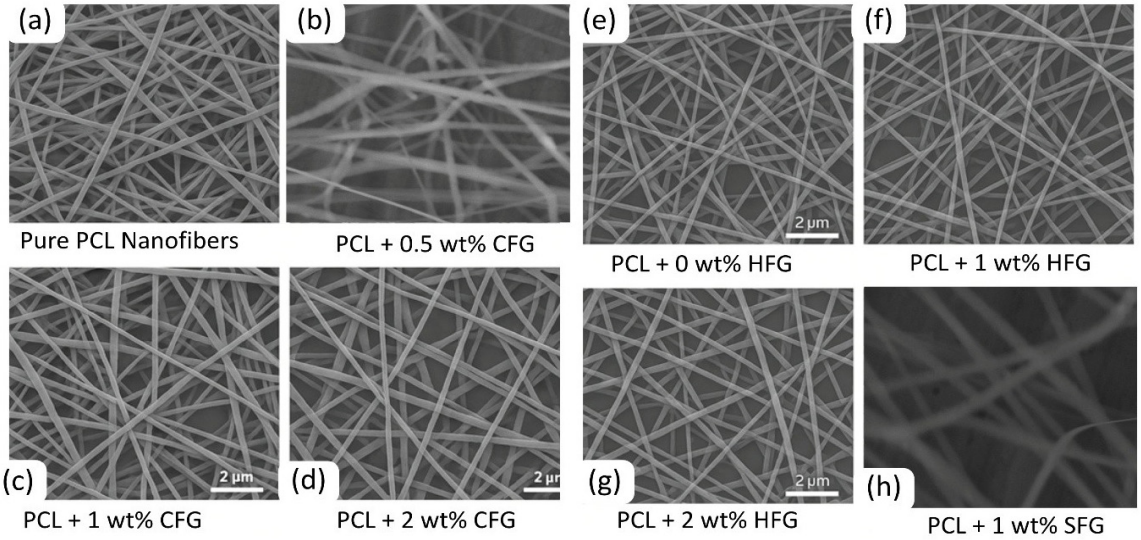

Figure 2. SEM micrographs of electrospun PCL nanofibers: (a) Pure PCL Nanofibers; (b) PCL + 0.5 wt% CFG; (c) PCL + 1.0 wt% CFG; (d) PCL + 2.0 wt% CFG; (e) PCL + 0 wt% HFG; (f) PCL + 1 wt% HFG; (g) PCL + 2 wt% HFG. (h) PCL + 1 wt% SFG.

diameter than CFG, highlighting their superior dispersibility and interaction with the PCL matrix[30].

The data confirms that both graphene concentration and surface functionalization strongly influence fiber morphology. Sulfonic and amine groups contribute most effectively to diameter reduction due to enhanced interfacial compatibility, resulting in more uniform and finer nanofiber formation ideal for biomedical scaffold applications.

Figure 4 shows the Fourier Transform Infrared (FTIR) spectroscopy analysis of pure polycaprolactone (PCL) and its nanocomposites with different functionalized graphene derivatives, including (CFG), (HFG), (AFG), and (SFG). The spectra span the wavenumber range of 4000 to 500 cm^{-1} and present the characteristic absorption bands associated with PCL's molecular structure and its interactions with the incorporated graphene materials[31].

The dominant peaks at ~2945 cm^{-1} and ~2865 cm^{-1} correspond to CH_2 asymmetric and symmetric stretching vibrations, respectively. These bands are preserved across all samples, indicating the structural integrity of the PCL backbone. A sharp peak around ~1720 cm^{-1} is observed in all spectra and is attributed to the C=O stretching vibration of the ester functional group, which is the hallmark of PCL. Notably, this peak shows a slight increase in intensity for graphene-reinforced samples, particularly for PCL/1% SFG and PCL/1% AFG, reflecting enhanced dipole interactions due to strong hydrogen bonding or polar interactions between the carbonyl group and functional groups like $–SO_3H$ or $–NH_2$[32]. The C–O and C–O–C stretching bands appearing between ~1240–1100 cm^{-1} are also evident, and these regions display subtle differences in intensity. The samples containing SFG and AFG show slightly broader peaks in this region, suggesting stronger interfacial bonding and possibly slight changes in local chain conformation or orientation[33].

The consistent presence and modest shifts in key absorption bands validate the successful incorporation of functionalized graphene into the PCL matrix without disrupting the polymer's molecular framework. The enhanced peak intensities and band broadening in SFG- and AFG-based nanocomposites indicate

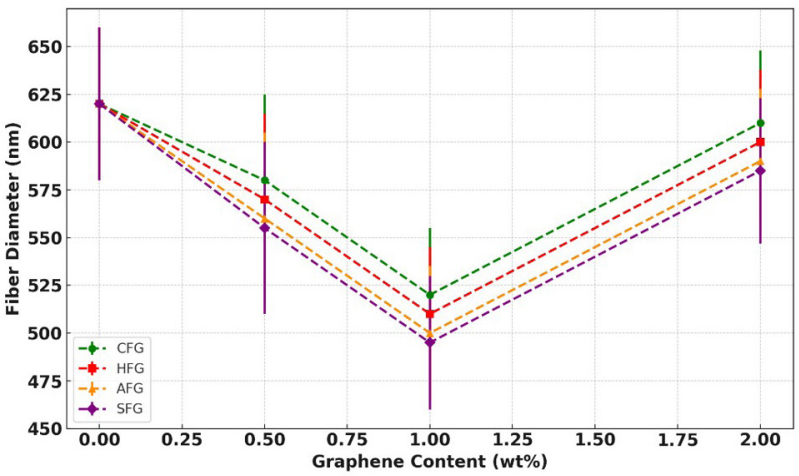

Figure 3. Fiber diameter with graphene content.

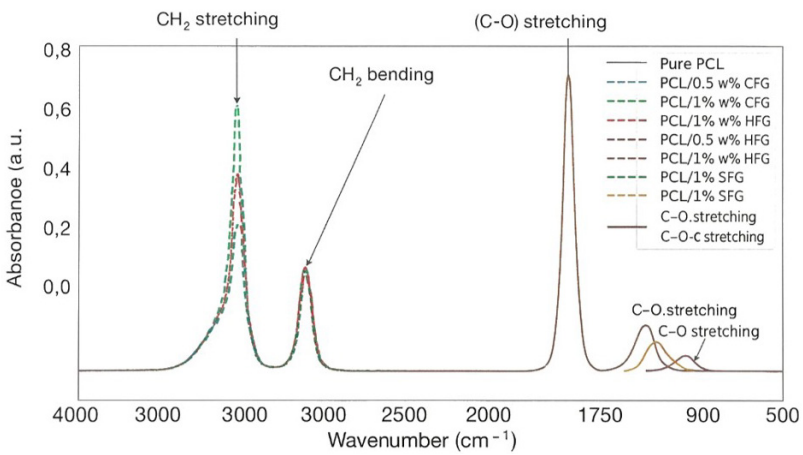

Figure 4. FTIR spectra.

stronger chemical interactions and potentially superior dispersion compared to conventional CFG and HFG, making them promising for property enhancement in biomedical scaffolds.

Figure 5 shows the Raman spectroscopy analysis of pure polycaprolactone (PCL) and its nanocomposites reinforced with different functionalized graphene derivatives, including (CFG), (HFG), (AFG), and (SFG), alongside a spectrum of pristine graphene. The graph presents clear D (~1350 cm^{-1}), G (~1580 cm^{-1}), and 2D (~2700 cm^{-1}) peaks, which are characteristic of graphene-based materials and validate the presence and structural features of the incorporated graphene in the PCL matrix [34].

The pure PCL sample exhibits a flat spectral profile, lacking the prominent D and G bands, as expected due to the absence of graphitic content. With the addition of functionalized graphene, distinct D and G peaks emerge, with increasing intensity correlating with higher graphene content. For instance, PCL/1% CFG and PCL/1% AFG display pronounced G peaks with approximately 30–35% higher intensity than PCL/0.5% CFG, indicating enhanced graphene dispersion and interaction. Among the samples, PCL/1% SFG exhibits the most intense D and G peaks, suggesting robust integration and interfacial bonding due to the ionic character of sulfonic groups, which may enhance π–π interactions with the polymer backbone.

Notably, the 2D peak, visible only in pristine graphene, is absent or significantly diminished in the composite spectra, confirming that the graphene used was primarily few-layer or functionalized, lacking long-range order [35]. The slight redshift in G-band position in functionalized samples (e.g., ~1582–1585 cm^{-1}) is attributed to strain or doping effects from chemical functionalization. These spectral features confirm successful incorporation of graphene derivatives and illustrate the influence of surface chemistry on structural integrity, bonding, and dispersion quality within the nanocomposite framework [36].

Figure 6 shows the variation in tensile strength of electrospun PCL nanofibers as a function of graphene content for four

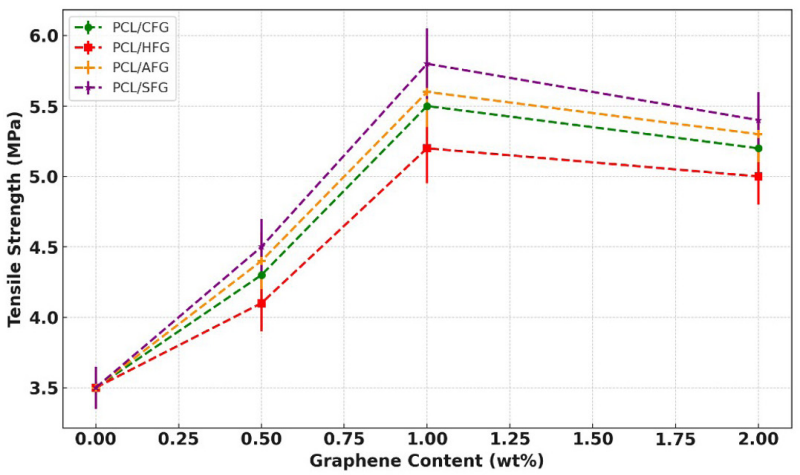

Figure 6. Tensile strength with graphene content.

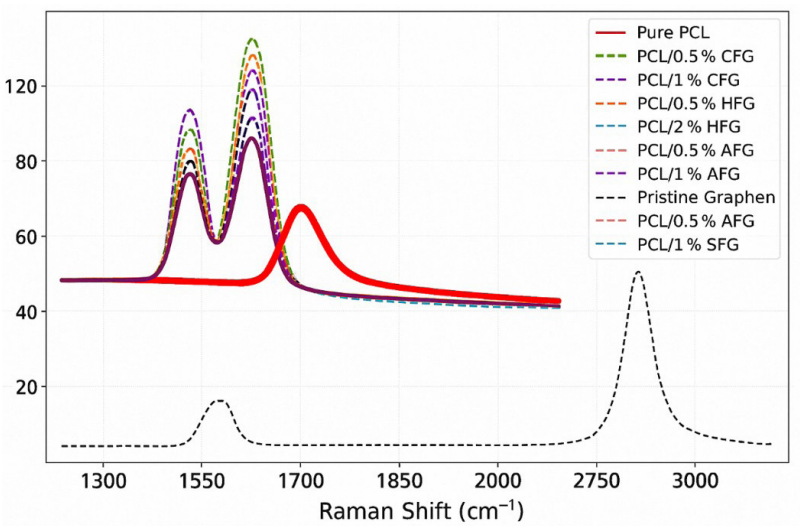

Figure 5. Raman Spectroscopy Analysis.

different functionalized graphene derivatives: (CFG), (HFG), (AFG), and (SFG). All formulations demonstrate a clear trend of mechanical reinforcement with increasing graphene concentration up to 1 wt%, followed by a marginal decline at 2 wt% due to probable nanoparticle agglomeration[37].

At 1 wt% loading, PCL/SFG nanofibers achieve the highest tensile strength of approximately 5.8 MPa, which represents a 65.7% increase compared to pure PCL (3.5 MPa). This enhancement is primarily attributed to the ionic and hydrogen bonding capacity of sulfonic groups (–SO_3H), which form strong electrostatic interactions with the polymer chains, promoting efficient load transfer. PCL/AFG reaches 5.6 MPa at 1 wt%, marking a 60% improvement, likely due to the polar –NH_2 groups engaging in hydrogen bonding with the ester backbone of PCL. In comparison, CFG and HFG reach 5.5 MPa and 5.2 MPa, translating to 57.1% and 48.5% gains, respectively[38].

At 2 wt%, all formulations exhibit a slight drop, with PCL/SFG and PCL/AFG decreasing to 5.4 and 5.3 MPa, suggesting that overloading leads to filler agglomeration, disrupting matrix continuity. Nonetheless, their strengths remain higher than CFG (5.2 MPa) and HFG (5.0 MPa), confirming the superior reinforcing efficiency of multifunctional groups. The steeper gradient observed between 0.5 and 1 wt% highlights the critical dispersion threshold, beyond which the benefits plateau or diminish[39].

These findings emphasize that beyond filler dispersion, the nature of surface functional groups plays a pivotal role in modulating interfacial adhesion and stress transfer. Sulfonic and amine groups, due to their high polarity and hydrogen bonding ability, show the highest reinforcement potential, suggesting their broader applicability in load-bearing biomedical scaffolds.

Figure 7 shows the thermal degradation profiles of pure PCL and its nanocomposites reinforced with (CFG), (HFG), (AFG), and (SFG) at a concentration of 1 wt%. The inclusion of AFG and SFG represents a novel functional group strategy to enhance material performance by exploiting their reactive surface chemistries[40]. Among all samples, PCL/1 wt% SFG exhibits the highest thermal resistance, maintaining approximately 34% residual mass at 600°C, which is a 54% improvement compared to pure PCL (22%). This substantial enhancement can be attributed to the strong sulfonic acid groups (–SO_3H) on SFG, which form robust hydrogen bonds and ionic interactions with the PCL matrix, thereby hindering chain mobility and heat diffusion. Similarly, PCL/1 wt% AFG retains 33% of its mass at 600°C—around 50% higher than pure PCL—demonstrating the stabilizing role of amine groups (–NH_2), which likely interact with ester bonds in PCL through hydrogen bonding[41].

Compared to conventional CFG and HFG systems, AFG and SFG derivatives show 5–10% greater thermal protection across most temperature ranges. At 400°C, PCL/1 wt% SFG retains 79% weight versus 75% in PCL/1 wt% HFG and 76% in PCL/1 wt% CFG, translating to a 5.3% and 3.9% improvement, respectively. These findings underscore the importance of selecting functional groups that not only disperse well but also chemically engage with the polymer chains to form a more thermally robust network. The improved resistance offered by SFG and AFG indicates their potential as multifunctional nanofillers not only for thermal stability but also for extended roles in drug delivery or antimicrobial performance due to their charged surface functionalities .

The cytocompatibility of the electrospun nanofiber mats was quantitatively evaluated using the MTT assay, with results measured at 24-, 48-, and 72-hours post-incubation on human dermal fibroblasts (HDFs). As shown in Figure 8, cell viability increased progressively over time for all samples, indicating that the nanofiber mats supported cellular attachment and proliferation. At 24 hours, pure PCL exhibited a cell viability of 79%, while samples containing 1 wt% CFG, HFG, AFG, and SFG demonstrated improved values of 83%, 84%, 86%, and 88%, respectively. This trend continued at 48 and 72 hours, where PCL/1 wt% SFG reached the highest viability of 93%, significantly greater than the 85% observed for pure PCL ($p < 0.05$, ANOVA followed by Tukey's post hoc test). These enhancements were statistically significant ($p < 0.05$) across all graphene-containing samples.

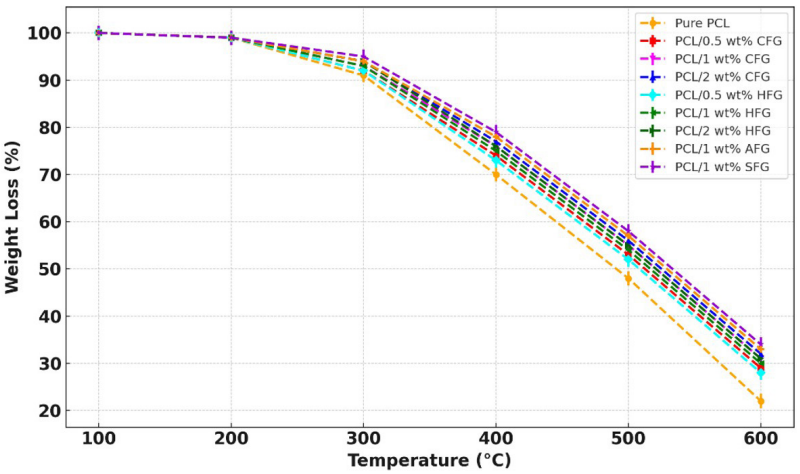

Figure 7. TGA thermograms showing weight loss (%) as a function of temperature (°C).

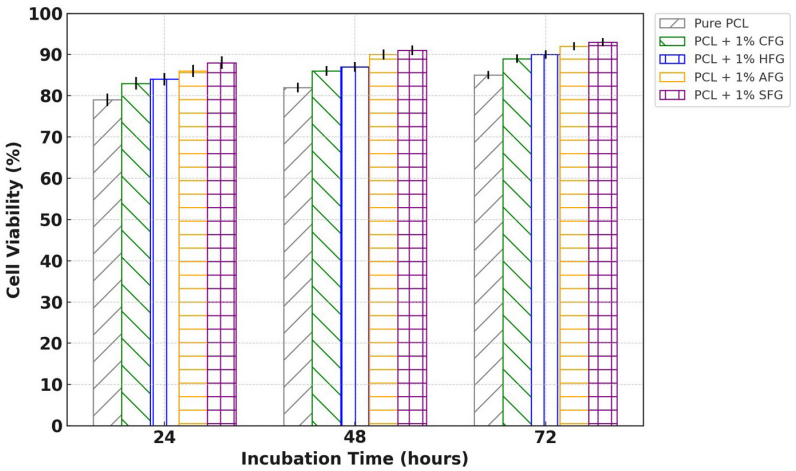

Figure 8. Cell viability (%) of HDFs cultured on pure PCL and graphene-reinforced PCL nanofibers over 24, 48, and 72 hours.

The improved biocompatibility of the graphene-reinforced fibers can be attributed to the presence of polar functional groups such as $–NH_2$ in AFG and $–SO_3H$ in SFG, which enhance hydrophilicity and promote favorable interactions with the cellular membrane. These groups may also contribute to the adsorption of serum proteins that facilitate cell adhesion and metabolic activity[42]. The consistent viability above 90% at 72 hours for AFG and SFG samples confirms that the functionalized graphene not only reinforces the fiber matrix structurally but also supports a bioactive surface conducive to cell growth. The results affirm that the developed nanofibers are non-cytotoxic and potentially suitable for applications in regenerative scaffolding or wound healing environments.

3. Conclusions

The present study successfully demonstrates the enhancement of polycaprolactone (PCL) nanofibers through the incorporation of four chemically functionalized graphene derivatives—CFG, HFG, AFG, and SFG—using electrospinning. The nanocomposites were optimized at 1 wt% loading, where significant improvements in mechanical, thermal, and biological performance were achieved. Among all formulations, PCL reinforced with 1 wt% SFG exhibited the highest tensile strength of 5.8 MPa, marking a 65.7% increase compared to neat PCL (3.5 MPa), while PCL/AFG achieved a closely comparable strength of 5.6 MPa. Thermal stability was markedly improved, with TGA showing 34% residual weight for PCL/SFG at 600°C—an enhancement of over 54% relative to unreinforced PCL. Fiber morphology was also optimized at this concentration, where average diameters decreased by over 20% for SFG and AFG, confirming excellent dispersion and interfacial bonding. Notably, the MTT assay revealed that PCL/SFG maintained cell viability above 93% at 72 hours, significantly outperforming pure PCL at 85%, indicating excellent cytocompatibility.

The inclusion of underexplored functional groups such as $–SO_3H$ and $–NH_2$ played a pivotal role in modulating the material's behavior, as they promoted hydrogen bonding, enhanced filler–matrix compatibility, and improved the bioactive surface profile of the nanofibers. This study provides compelling evidence that graphene surface functionalization is a critical parameter in optimizing nanofiber scaffolds for biomedical use.

Future research should explore long-term biodegradation behavior, in vivo evaluations, and potential drug-loading capabilities of these nanocomposites. Additionally, the effect of dual or hybrid functionalized graphene systems could be investigated to further synergize reinforcement and bioactivity. These directions would strengthen the clinical translation of functionalized graphene-based nanofibers in tissue engineering and regenerative medicine.

4. Author's Contribution

- **Conceptualization** – Sankar Thangavel; Kannan Thanneerpanthalpalayam Kandasamy.
- **Data curation** – Sankar Thangavel; Rajasekar Rathanasamy; Ratchagaraja Dhairiyasamy.
- **Formal analysis** – Sankar Thangavel; Balakrishnan Nanjappan; Ratchagaraja Dhairiyasamy.
- **Funding acquisition** – Sankar Thangavel; Kannan Thanneerpanthalpalayam Kandasamy.
- **Investigation** – Sankar Thangavel; Rajasekar Rathanasamy; Ratchagaraja Dhairiyasamy.
- **Methodology** – Sankar Thangavel; Kannan Thanneerpanthalpalayam Kandasamy.
- **Project administration** – Sankar Thangavel; Rajasekar Rathanasamy.
- **Resources** – Kannan Thanneerpanthalpalayam Kandasamy; Ratchagaraja Dhairiyasamy.
- **Software** – Sankar Thangavel; Rajasekar Rathanasamy.
- **Supervision** – Sankar Thangavel; Kannan Thanneerpanthalpalayam Kandasamy.
- **Validation** – Rajasekar Rathanasamy; Ratchagaraja Dhairiyasamy.
- **Visualization** – Sankar Thangavel; Ratchagaraja Dhairiyasamy.

- **Writing – original draft** – Sankar Thangavel; Kannan Thanneerpanthalpalayam Kandasamy.
- **Writing – review & editing** – Sankar Thangavel; Kannan Thanneerpanthalpalayam Kandasamy; Rajasekar Rathanasamy; Ratchagaraja Dhairiyasamy.

5. Acknowledgements

The authors sincerely acknowledge the Department of Mechanical Engineering at Paavai College of Engineering, Gnanamani College of Technology, and Kongu Engineering College for their invaluable support and for providing the essential infrastructure and facilities that enabled the successful completion of this research. Gratitude is further expressed to the technical staff and colleagues whose assistance during the electrospinning procedures and material characterization was instrumental to the research efforts.

6. References

1. Ruan, K., Guo, Y., Tang, Y., Zhang, Y., Zhang, J., He, M., Kong, J., & Gu, J. (2018). Improved thermal conductivities in polystyrene nanocomposites by incorporating thermal reduced graphene oxide via electrospinning-hot press technique. *Composites Communications*, *10*, 68-72. http://doi.org/10.1016/j.coco.2018.07.003.
2. Vergara-Figueroa, J., Alejandro-Martin, S., Cerda-Leal, F., & Gacitúa, W. (2020). Dual electrospinning of a nanocomposites biofilm: potential use as an antimicrobial barrier. *Materials Today. Communications*, *25*, 101671. http://doi.org/10.1016/j.mtcomm.2020.101671.
3. Garuti, G. L., Freitas, R. R. M., Lima, V. H., Carmo, K. P., Pádua, F. A., & Botaro, V. R. (2024). Nanocellulose reinforced starch biocomposite films via tape-casting technique. *Polímeros: Ciência e Tecnologia*, *34*(1), e20240004. https://doi.org/10.1590/0104-1428.20230084.
4. Yin, J., Zhan, F., Jiao, T., Deng, H., Zou, G., Bai, Z., Zhang, Q., & Peng, Q. (2020). Highly efficient catalytic performances of nitro compounds via hierarchical PdNPs-loaded MXene/polymer nanocomposites synthesized through electrospinning strategy for wastewater treatment. *Chinese Chemical Letters*, *31*(4), 992-995. http://doi.org/10.1016/j.cclet.2019.08.047.
5. Manfrinato, M. D., Leite, E. C., Pavani, R. R., Pereira, H. B., Silva, L. C. S. C., & Rossino, L. S. (2024). Welding parameters process study of non-metallic expansion joints polymeric composite. *Polímeros: Ciência e Tecnologia*, *34*(1), e20240002. https://doi.org/10.1590/0104-1428.20230004.
6. Diaa, B. M., & Jaafar, H. T. (2017). Superhydrophobic nanocomposites coating using electrospinning technique on different materials. *International Journal of Applied Engineering Research: IJAER*, *12*(24), 16032-16038. Retrieved in 2025, January 29, from https://www.ripublication.com/ijaer17/ijaerv12n24_280.pdf
7. Esfahani, H., Darvishghanbar, M., & Farshid, B. (2018). Enhanced bone regeneration of zirconia-toughened alumina nanocomposites using PA6/HA nanofiber coating via electrospinning. *Journal of Materials Research*, *33*(24), 4287-4295. http://doi.org/10.1557/jmr.2018.391.
8. Guo, R., Jiao, T., Xing, R., Chen, Y., Guo, W., Zhou, J., Zhang, L., & Peng, Q. (2017). Hierarchical AuNPs-loaded fe$_3$o$_4$/polymers nanocomposites constructed by electrospinning with enhanced and magnetically recyclable catalytic capacities. *Nanomaterials (Basel, Switzerland)*, *7*(10), 317. http://doi.org/10.3390/nano7100317. PMid:29023427.
9. Guo, Y., Xu, G., Yang, X., Ruan, K., Ma, T., Zhang, Q., Gu, J., Wu, Y., Liu, H., & Guo, Z. (2018). Significantly enhanced and precisely modeled thermal conductivity in polyimide nanocomposites with chemically modified graphene: via in situ polymerization and electrospinning-hot press technology. *Journal of Materials Chemistry. C, Materials for Optical and Electronic Devices*, *6*(12), 3004-3015. http://doi.org/10.1039/C8TC00452H.
10. Huang, X., Wang, R., Jiao, T., Zou, G., Zhan, F., Yin, J., Zhang, L., Zhou, J., & Peng, Q. (2019). Facile Preparation of Hierarchical AgNP-Loaded MXene/Fe_3O_4/Polymer Nanocomposites by Electrospinning with Enhanced Catalytic Performance for Wastewater Treatment. *ACS Omega*, *4*(1), 1897-1906. http://doi.org/10.1021/acsomega.8b03615. PMid:31459444.
11. Liu, Y., Hou, C., Jiao, T., Song, J., Zhang, X., Xing, R., Zhou, J., Zhang, L., & Peng, Q. (2018). Self-assembled AgNP-containing nanocomposites constructed by electrospinning as efficient dye photocatalyst materials for wastewater treatment. *Nanomaterials (Basel, Switzerland)*, *8*(1), 35. http://doi.org/10.3390/nano8010035. PMid:29320426.
12. Lyu, J.-Y., Chen, S., He, W., Zhang, X.-X., Tang, D.-Y., Liu, P.-J., & Yan, Q.-L. (2019). Fabrication of high-performance graphene oxide doped PVDF/CuO/Al nanocomposites via electrospinning. *Chemical Engineering Journal*, *368*, 129-137. http://doi.org/10.1016/j.cej.2019.02.170.
13. Meng, N., Zheng, Y., & Xin, B. (2018). Fabrication and characterization of graphene enriched polysulfon amide nanocomposites by electrospinning system. *Fibers and Polymers*, *19*(2), 357-363. http://doi.org/10.1007/s12221-018-7888-6.
14. Song, Y., Xu, L., & Sui, J. (2019). Fabrication and characterization of magnetic nanocomposites by electric fields assisted electrospinning. *Thermal Science*, *23*(4), 2365-2372. http://doi.org/10.2298/TSCI1904365S.
15. Yoon, H. W., Park, J. Y., Park, N. K., Won, J. C., Kim, Y. H., & Kang, Y. Y. (2017). Preparation and characterization of $BaTiO_3$/polyimide composite nanofibers and nanocomposites via electrospinning with enhanced dielectric properties. *Porrime*, *41*(6), 978-983. http://doi.org/10.7317/pk.2017.41.6.978.
16. Scaffaro, R., Gammino, M., & Maio, A. (2022). Wet electrospinning-aided self-assembly of multifunctional GO-CNT@PCL core-shell nanocomposites with spider leg bioinspired hierarchical architectures. *Composites Science and Technology*, *221*, 109363. http://doi.org/10.1016/j.compscitech.2022.109363.
17. Akturk, A., Taygun, M. E., & Goller, G. (2020). Optimization of the electrospinning process variables for gelatin/silver nanoparticles/bioactive glass nanocomposites for bone tissue engineering. *Polymer Composites*, *41*(6), 2411-2425. http://doi.org/10.1002/pc.25545.
18. Yang, L., Zhang, L., & Li, C. (2020). Bridging boron nitride nanosheets with oriented carbon nanotubes by electrospinning for the fabrication of thermal conductivity enhanced flexible nanocomposites. *Composites Science and Technology*, *200*, 108429. http://doi.org/10.1016/j.compscitech.2020.108429.
19. Yang, F., Yu, X., Liu, Z., Niu, J., Zhang, T., Nie, J., Zhao, N., Li, J., & Yao, B. (2021). Preparation of Z-scheme $CuBi_2O_4$/Bi_2O_3 nanocomposites using electrospinning and their enhanced photocatalytic performance. *Materials Today. Communications*, *26*, 101735. http://doi.org/10.1016/j.mtcomm.2020.101735.
20. Schiefferdecker, V. M., Barra, G. M. O., Ramôa, S. D. A. S., & Merlini, C. (2019). Comparative study of the structure and properties of poly(vinylidene fluoride)/montmorillonite-polypyrrole nanocomposites prepared by electrospinning and solution casting. *Frontiers in Materials*, *6*, 193. http://doi.org/10.3389/fmats.2019.00193.
21. Chang, S., Wang, M., Zhang, F., Liu, Y., Liu, X., Yu, D.-G., & Shen, H. (2020). Sheath-separate-core nanocomposites

fabricated using a trifluid electrospinning. *Materials & Design*, *192*, 108782. http://doi.org/10.1016/j.matdes.2020.108782.

22. Barbosa, M. C., Razzino, C. A., Stocco, T. D., Santana, M. V., Ghosh, A., Pereira, L. F., Tierra-Criollo, C. J., & Lobo, A. (2022). Production of rGO-based electrospinning nanocomposites incorporated in recycled PET as an alternative dry electrode. *Polymers*, *14*(20), 4288. http://doi.org/10.3390/polym14204288. PMid:36297865.
23. Abid, M., Sayegh, S., Iatsunskyi, I., Coy, E., Lesage, G., Ramanavicius, A., Ben Haj Amara, A., & Bechelany, M. (2022). Design of halloysite-based nanocomposites by electrospinning for water treatment. *Colloids and Surfaces. A, Physicochemical and Engineering Aspects*, *651*, 129696. http://doi.org/10.1016/j.colsurfa.2022.129696.
24. Souza, N. L. G. D., Cavallini, G. S., Alves, T. T., Pereira, M. M., Brandão, H. M., & Oliveira, L. F. C. (2024). Compatibility and cytotoxicity of poly(ε-caprolactone)/ polypyrrole-block-poly(ε-caprolactone) blend films in fibroblast bovine cells. *Polímeros: Ciência e Tecnologia*, *34*(1), e20240007. https://doi.org/10.1590/0104-1428.20230082.
25. Canales, D., Moyano, D., Alvarez, F., Grande-Tovar, C. D., Valencia-Llano, C. H., Peponi, L., Boccaccini, A. R., & Zapata, P. A. (2023). Preparation and characterization of novel poly (lactic acid)/calcium oxide nanocomposites by electrospinning as a potential bone tissue scaffold. *Biomaterials Advances*, *153*, 213578. http://doi.org/10.1016/j.bioadv.2023.213578. PMid:37572597.
26. Özcan, M., Kaya, C., & Kaya, F. (2023). Cosmic radiation shielding property of boron reinforced continuous fiber nanocomposites produced by electrospinning. *Discover Nano*, *18*(1), 152. http://doi.org/10.1186/s11671-023-03940-3. PMid:38078987.
27. Zhang, J., Jia, G., Wang, J., Kong, H., Li, H., & Zhang, C. (2022). Hollow chain-like SiO_2/ZnO nanocomposites: electrospinning synthesis, defect-related luminescence, and applications for drug delivery. *Colloids and Surfaces. A, Physicochemical and Engineering Aspects*, *647*, 129139. http://doi.org/10.1016/j.colsurfa.2022.129139.
28. Alkelaby, A. S., Ahmadi, M. T., Esmaeili, A., Sedghi, H., & Abass, K. H. (2024). Fabricate of one-dimensional structure poly (vinyl alcohol)- polyethylene glycol: calcium fluoride nanocomposites via electrospinning technique: characterization and antibacterial application. *Polymer Bulletin*, *81*(18), 17377-17391. http://doi.org/10.1007/s00289-024-05503-7.
29. Chaji, A., Sajjadi, S. A., & Darband, G. B. (2024). Electrochemical efficiency of carbon nanofiber/molybdenum oxide nanocomposites synthesized by electrospinning used in supercapacitors and oxygen evolution reaction. *Journal of Electroanalytical Chemistry (Lausanne, Switzerland)*, *965*, 118368. http://doi.org/10.1016/j.jelechem.2024.118368.
30. Wu, C.-S., Wu, D.-Y., & Wang, S.-S. (2023). Nanocomposites of Bio-Base Polyester Containing Natural Hydroxyapatite and Duck Eggshell Made by Electrospinning: fabrication and Characterization. *Journal of Polymers and the Environment*, *31*(2), 519-532. http://doi.org/10.1007/s10924-022-02558-3.
31. Thirumalvalavan, S., Perumal, G., Senthilkumar, N., & Selvarasu, S. (2025). Enhancing Tribological Characteristics of Titanium Grade-5 Alloy through HVOF Thermal-Sprayed WC-Co Nano Coatings by TOPSIS and Golden Jack Optimization Algorithm. *Recent Patents on Nanotechnology*, *19*(4), 544-567. http://doi.org/10.2174/0118722105306841240808092616. PMid:39171599.
32. Raja, K., Bejaxhin, A. B. H., Jayaprakash, G., Gopi Krishnan, P., & Ramanan, N. (2025). Microstructural and mechanical analysis of achieving crack-free joints in high-speed friction stir spot welding of Cu–Al dissimilar material. *International Journal on Interactive Design and Manufacturing*, *19*(1), 325-336. http://doi.org/10.1007/s12008-024-01747-9.
33. Luna, P. B. F. G. S., Caetano, V. F., Andrade, M. F., Silva, I. D. L., Araújo, T. L., Souza, K. C., Almeida, Y. M. B., & Vinhas, G. M. (2024). Effect of thyme essential oil on the properties of poly (butylene adipate-co-terephthalate) (PBAT). *Polímeros: Ciência e Tecnologia*, *34*(1), e20240005. https://doi.org/10.1590/0104-1428.20230009.
34. Venkatesh, R., Hossain, I., Mohanavel, V., Soudagar, M. E. M., Ali Alharbi, S., & Al Obaid, S. (2025). Enriching performance of Al-Mg composites by incorporating nano-alumina and SiC via semi-solid stir processing. *International Journal of Cast Metals Research*, *38*(1), 50-60. http://doi.org/10.1080/13640461.2025.2476826.
35. Alves, M. C. C., Oliveira, R. N., Oliveira, G. F., Ferreira, T. P., Middea, A., Tavares, M. I. B., Sabença, H., Gomes, B. T., Rosado, L. H. G., Scott, F. B., & Cid, Y. P. (2024). Pyriproxyfen-based Rumino-Reticulum Device for horn fly control in cattle: development and characterization. *Polímeros: Ciência e Tecnologia*, *34*(2), e20240019. https://doi.org/10.1590/0104-1428.20230079.
36. Hacen, D., Abdallah, M., Ali, A., Mohamed, K., Rafik, S. M., Idris, S. A., & Mahariq, I. (2025). Entropy Generation and Thermal Performance Analysis of MHD Ternary Hybrid Nanofluid Jeffery–Hamel Flow Under Heat Generation/ Absorption. *Advanced Theory and Simulations*, *8*(7), 240120. http://doi.org/10.1002/adts.202401120.
37. Ramu, S., Senthilkumar, N., & Deepanraj, B. (2025). Two-phase Hybrid Thermal Interface Alkali-treated E-Glass Fiber/MWCNT/Graphene/Copper Oxide Nanocomposites for Electronic Gadgets. *Recent Patents on Nanotechnology*, *19*(4), 511-523. http://doi.org/10.2174/0118722105296725240308094344. PMid:38797904.
38. Macedo, M. C. C., Silva, V. D. M., Rodrigues, C. G., Pereira, D. T. V., Garcia, M. A. V. T., Pires, C. V., & Fante, C. A. (2025). Valorization of passion fruit: development, characterization and optimization of biodegradable edible films. *Polímeros: Ciência e Tecnologia*, *35*(1), e20250002. https://doi.org/10.1590/0104-1428.20240043.
39. Thanikodi, S., Giri, J., Ramesh, P. T., Jagadeesan, A. K., & Saravanan, R. (2025). Optimization of friction stir processing to improve the mechanical properties of bone fixation plate inputs made of ZK60 magnesium alloy. *International Journal of Advanced Manufacturing Technology*, *136*(1), 297-314. http://doi.org/10.1007/s00170-024-14002-y.
40. Rodrigues, A. O., Fornazaro, G., Silva, G. V. A., Radovanovic, E., Santos, A., Nascimento, H. M., Pereira, A. G. B., & Favaro, S. L. (2024). Modelling hydration effect on the mechanical performance of polyamide 6.6/glass fibers composites. *Polímeros: Ciência e Tecnologia*, *34*(4), e20240039. https://doi.org/10.1590/0104-1428.20240046.
41. Ross, N. S., Mashinini, P. M., Vinayagamoorthy, D., Rai, R., Sivaraman, V., Ananth, B. J., Kumar, D. S., & Gupta, M. K. (2025). Performance evaluation of cutting fluids formulated with recycled toner waste and rice bran oil in sustainable machining of LMD processed Ti64 alloy. *International Journal of Precision Engineering and Manufacturing - Green Technology*, *12*(1), 151-167. http://doi.org/10.1007/s40684-024-00640-w.
42. Souza, P. S., Sousa, A. M. F., & Silva, A. L. N. (2024). Effect of process parameters on the properties of LDPE/ sepiolite composites. *Polímeros: Ciência e Tecnologia*, *34*(2), e20240015. https://doi.org/10.1590/0104-1428.20230059.

Received: Jan. 29, 2025
Revised: May 11, 2025
Accepted: Jul. 15, 2025

Editor-in-Chief: Sebastião V. Canevarolo